

THE HYDROGEN EPOCH OF REIONIZATION ARRAY DISH: CHARACTERIZATION WITH ELECTROMAGNETIC SIMULATIONS

EWALL-WICE AARON^{1,2}, BRADLEY RICHARD^{3,4}, JACQUELINE HEWITT^{1,2}, ALI S. ZAKI⁵, BOWMAN JUDD⁶, CHENG CARINA⁵, NEBEN ABRAHAM^{1,2}, PARSONS AARON⁵, PATRA NIPANJANA⁵, THYAGARAJAN NITHYANANDAN⁶

Draft version October 24, 2015

ABSTRACT

Using electromagnetic simulations, we assess the spectral properties of the antenna element of the Hydrogen Epoch of Reionization Array (HERA) in order to both establish a specification for the degree of spectral structure that is permissible to sufficiently isolate foregrounds and allow a detection of the cosmological 21 cm signal and verify direct laboratory measurements of the dish characteristics. We find that our simulations are in good agreement with field measurements. Using simulations of foregrounds, we find that the ≈ -40 dB response at 60 ns of the HERA dish is sufficient to isolate the cosmological 21 cm signal $\approx 0.2 \text{ hMpc}^{-1}$ at $z \approx 8.5$ and obtain a high signal to noise detection of the power spectrum.

1. INTRODUCTION

Observations of the redshift 21 cm radiation neutral hydrogen in the intergalactic medium (IGM) have the potential to illuminate the hitherto unobserved *dark ages* and *cosmic dawn*, revolutionizing our understanding of the first UV and X-ray sources in the universe and how their properties influenced galactic evolution (see Furlanetto et al. (2006), Morales & Wyithe (2010), and Pritchard & Loeb (2012) for reviews). As of now, two major experimental endeavors are underway to make a first detection of the 21 cm signal with most focusing on the Epoch of Reionization (EoR) in which UV photons from early galaxies transformed the hydrogen in the universe from neutral to ionized. The first involves measuring the sky-averaged global signal and is being pursued by experiments such as EDGES (Bowman & Rogers 2010), LEDA (Greenhill & Bernardi 2012), DARE (Burns et al. 2012), SciHi (Voytek et al. 2014), and BIGHORNS (Sokolowski et al. 2015) coming online in their planning stages or taking data. The second attempts to observe spatial fluctuations in the 21 cm emission using radio interferometers. As of now, a first generation of interferometry experiments are taking data in an attempt to make a first statistical detection of the power spectrum of 21 cm brightness temperature fluctuations. These include the Giant Metrewave Telescope (GMRT) (Paciga et al. 2013), the Low Frequency Array (LOFAR), (van Haarlem et al. 2013), the Murchison Widefield Array (?) and the Precision Array for Probing the Epoch of Reionization (PAPER) (Parsons et al. 2010).

The primary obstacle to obtaining a high redshift detection of the cosmological signal through both of these methods is the existence of foregrounds that are $\sim 10^5 - 10^6$ times brighter. While requiring much greater sensitivity to global-signal experiments, interferometers

have the advantage that these spectrally smooth foregrounds naturally avoid a significant region of k -space, known as the *EoR window*, occupying a region known as the *wedge* (Datta et al. 2010; Vedantham et al. 2012; Parsons et al. 2012; Thyagarajan et al. 2013; Liu et al. 2014a,b), however any structure in the frequency response of the instrument has the potential to leak foregrounds into the EoR window, masking our signal. Indeed, low level spectral structures in the analogue and digital signal chains on the initial buildup of the MWA are proving to be a significant obstacle (Dillon et al. 2015; Ewall-Wice et al. submitted 2015; Beardsley et al. in preparation).

While, in principle, spectral structure in the bandpass of the instrument may be removed in calibration, simulations show that any mismodeling of emission and the primary beam, potentially below the confusion limit, will mix the significant spectral structure on long baselines into short ones, masking the signal entirely (Barry et al. in preparation). While redundant calibration (Wieringa 1992; Liu & Tegmark 2011; Zheng et al. 2014) is able to calibrate the independent of a detailed model of the sky, any direction-dependent chromatic structure in the primary beam of the instrument introduces additional degrees of freedom that must be modeled, potentially leading to signal loss and the introduction of spurious spectral structure due to unmodeled foregrounds in long baselines. Because of our limited knowledge of foregrounds at low-frequency and the fidelity of calibration algorithms, the only sure way of building an instrument that will guarantee a detection of the redshifted 21 cm emission is to design it such that all spectral structure in the signal chain is limited to a finite region of delay space, well below the wedge.

The Hydrogen Epoch of Reionization Array (HERA) is an instrument currently taking first observations in the Karoo in South Africa with the ultimate goal of detecting the power spectrum of 21 cm brightness temperature fluctuations at high signal-to-noise (SNR) (Poher et al. 2014). A central principle in HERA's design is that it be calibration fail-safe such that a detection of the signal is guaranteed, even if the chromaticity of the instrument is not calibrated out. This paper and its com-

¹ MIT Kavli Institute for Cosmological Physics

² MIT Dept. of Physics

³ National Radio Astronomy Obs., Charlottesville VA

⁴ Dept. of Astronomy, U. Virginia, Charlottesville VA

⁵ Astronomy Dept. U. California, Berkeley CA

⁶ School of Earth and Space Exploration, Arizona State U., Tempe AZ



FIG. 1.— The HERA primary antenna element—one of 19 undergoing currently taking the first observations in the Karoo in South Africa. The antenna consists of a sleeved dipole suspended within a 2 m diameter skirt, five meters above the ground at the focal point of a 14 m diameter dish.

panions (Neben et al. submitted; Patra et al. submitted; Thyagarajan et al. submitted) describe a multifaceted approach to establishing a stringent specification on the spectral structure permissible for HERA to be calibration fail-safe and determine to what extent its design meets these requirements. We accomplish this by establishing a spec with simulations of foregrounds (?) and verifying that HERA primary antenna element meets this spec with reflectometry (Patra et al. submitted) and Orbcomm beam mapping (Neben et al. submitted). These measurements are verified with detailed electromagnetic simulations which we describe in this work.

This paper is organized as follows. In § 2 we lay out our analytic framework for describing the impact of reflections and spectral structure on foreground leakage in delay-transform power spectra. In § 3 we describe our electromagnetic simulations of the HERA dish element. In § 4 we compare our simulation results to direct measurements of the primary dish element and in § 5 we apply our electromagnetic simulation results to simulations of foregrounds to determine the extent that the HERA dish’s chromatic structure pollutes the EoR window and their impact on HERA’s overall sensitivity. We conclude in § 6.

2. THE IMPACT OF REFLECTIONS ON DELAY-TRANSFORM POWER SPECTRA

In this section, we show how reflections in the analogue signal path of an antenna lead to foreground contamination of the EoR window. HERA’s primary antenna element consists of a sleeved dipole element suspended 5 m above the focus of a 14 m diameter parabolic dish (Fig. 1).

We show in Appendix A that if an astronomical radio signal with time dependence at the location of the feed, $s(\hat{\mathbf{k}}, t)$, experience reflections within the dish such that the voltage recorded in the feed is

$$v(t) = \sum_n r_n(\hat{\mathbf{k}}) s(\hat{\mathbf{k}}, t - \tau_n) \quad (1)$$

Than the resulting visibilities obtained by cross correlat-

ing antenna i and antenna j are given by

$$V'_{ij}(f) = \sum_{m,n} \int d\Omega R_{mn}(\hat{\mathbf{k}}) e^{2\pi i \Delta\tau_{mn} f} e^{2\pi i \mathbf{u}_{ij} \cdot \hat{\mathbf{k}}} I(f, \hat{\mathbf{s}}), \quad (2)$$

where $R_{mn}(\hat{\mathbf{s}}) = r_m r_n^*$, $I(f, \hat{\mathbf{s}})$ is the intensity of the signal on the sky, and can be decomposed into foregrounds and signal

$$I(f, \hat{\mathbf{s}}) = I_{fg}(f, \hat{\mathbf{s}}) + I_{21}(f, \hat{\mathbf{s}}) \quad (3)$$

While I_{fg} is on the order of 10^6 times larger than I_{21} , the continuum emission from foregrounds is expected to be spectrally smooth. Hence, a *delay transform* defined by

$$\tilde{V}_{ij}(\tau) = \int df e^{-2\pi i \tau f} V'_{ij}(f) \quad (4)$$

should, in principle, separate the foregrounds from the signal with foregrounds occupying the wedge. However, the introduction of the chromatic $e^{2\pi i \Delta\tau_{mn}}$ terms leads to foreground contamination being convolved out to higher delays.

$$\tilde{V}'_{ij}(\tau) = \sum_{m,n} \tilde{V}_{ij,FG}^{mn}(\tau - \Delta\tau_{mn}) + \tilde{V}_{ij,21}^{mn}(\tau - \Delta\tau_{mn}) \quad (5)$$

where V_{ij}^{mn} is a visibility resulting from the effective primary beam, $R_{mn}(\hat{\mathbf{k}})$, at delay $\Delta\tau_{mn}$ induced by the reflections.

$$V_{ij}^{mn} = \int d\Omega R_{mn}(\hat{\mathbf{s}}) I(f, \hat{\mathbf{s}}) e^{2\pi i \mathbf{u}_{ij} \cdot \hat{\mathbf{s}}} \quad (6)$$

The delay transform power spectrum estimate, \hat{P} , is proportional to $|\tilde{V}'_{ij}|^2$, hence

$$\begin{aligned} \hat{P} \propto & |\tilde{V}_{ij,FG}(\tau)|^2 + |\tilde{V}_{ij,21}(\tau)|^2 + 2\text{Re}(\tilde{V}_{ij,21}(\tau) \tilde{V}_{ij,FG}^*(\tau)) \\ & + \sum_{|\Delta\tau_{mn}| > 0} 2\text{Re} \left[\tilde{V}_{ij}^*(\tau) \tilde{V}_{ij}^{mn}(\tau - \Delta\tau_{mn}) \right] \\ & + \sum_{\substack{|\Delta\tau_{op}| > 0 \\ |\Delta\tau_{mn}| > 0}} \tilde{V}_{ij}^{mn}(\tau - \Delta\tau_{mn}) \tilde{V}_{ij}^{op*}(\tau - \Delta\tau_{op}) \end{aligned} \quad (7)$$

In the absence of reflections, only the top line of equation 7 would enter the delay power spectrum estimate. The following lines involve the translation of the signal (including foregrounds and signal) out to the delay of each reflection and weighted by the effective primary beam of the reflection. Since each translated visibility is intrinsically $\sim 10^6$ times brighter than the signal, any reflection with a delay large enough to place it within the EoR window, must be sufficiently attenuated by $R_{mn}(\hat{\mathbf{k}})$. The precise degree of attenuation is determined in (Thyagarajan et al. submitted) using simulations of foregrounds and noise and sets the spec for our antenna. In this paper, we study $R_{mn}(\hat{\mathbf{k}})$ for the HERA antenna element to verify that it both meets the spec and agrees with direct measurements of the antenna element with refelctometry (Patra et al. submitted) and Orbcomm measurements (Neben et al. submitted).

3.1. The Simulations

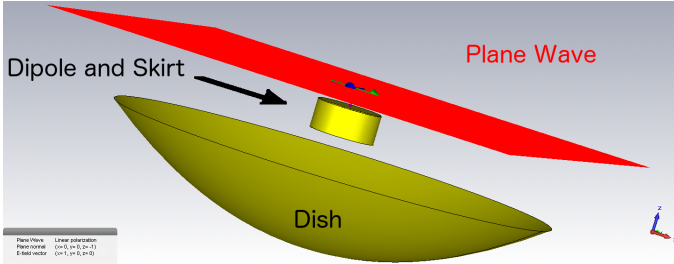


FIG. 2.— A rendering of our time domain simulation at $t = 0$, demonstrating the geometry and setup of our electromagnetic simulation. The plane wave is started just above the feed (red plane).

3. ELECTROMAGNETIC SIMULATIONS OF THE HERA DISH ELEMENT

In Fig. 2 we show the geometry of the electromagnetic simulation. Rich: fill in the details here

3.2. Deconvolving the Response Function

In our simulation, we obtain the voltage at the feed output as a function of time which we will call $v_{out}(t)$. It is related to the input lane wave through the equation

$$v_{out}(t) = \sum_n r_n(\theta = 0)v_{in}(t - \tau_n) \quad (8)$$

which is essentially a convolution in time of $r_n(\theta = 0)$ with the input plane wave

4. COMPARING SIMULATIONS RESULTS TO MEASUREMENTS

5. THE EFFECT OF THE HERA DISH CHROMATICITY ON FOREGROUND LEAKAGE AND SENSITIVITY

6. CONCLUSIONS

REFERENCES

- Barry et al. in preparation
 Beardsley et al. in preparation
 Bowman, J. D., & Rogers, A. E. E. 2010, Nature, 468, 796
 Burns, J. O., et al. 2012, Advances in Space Research, 49, 433
 Datta, A., Bowman, J. D., & Carilli, C. L. 2010, ApJ, 724, 526
 Dillon, J. S., et al. 2015, Phys. Rev. D, 91, 123011
 Ewall-Wice, A., et al. submitted 2015, Submitted to MNRAS
 Furlanetto, S. R., Oh, S. P., & Briggs, F. H. 2006, Phys. Rep., 433, 181
 Greenhill, L. J., & Bernardi, G. 2012, ArXiv e-prints
 Liu, A., Parsons, A. R., & Trott, C. M. 2014a, Phys. Rev. D, 90, 023018
 —. 2014b, Phys. Rev. D, 90, 023019
 Liu, A., & Tegmark, M. 2011, Phys. Rev. D, 83, 103006
 Morales, M. F., & Wyithe, J. S. B. 2010, ARA&A, 48, 127
 Neben et al. submitted, ApJ
 Paciga, G., et al. 2013, MNRAS, 433, 639
 Parsons, A. R., Pober, J. C., Aguirre, J. E., Carilli, C. L., Jacobs, D. C., & Moore, D. F. 2012, ApJ, 756, 165
 Parsons, A. R., et al. 2010, AJ, 139, 1468
 Patra et al. submitted, ApJ
 Pober, J. C., et al. 2014, ApJ, 782, 66
 Pritchard, J. R., & Loeb, A. 2012, Reports on Progress in Physics, 75, 086901
 Sokolowski, M., et al. 2015, PASA, 32, 4
 Thyagarajan, N., et al. 2013, ApJ, 776, 6
 Thyagarajan et al. submitted, ApJ
 van Haarlem, M. P., et al. 2013, A&A, 556, A2
 Vedantham, H., Udaya Shankar, N., & Subrahmanyan, R. 2012, ApJ, 745, 176
 Voytek, T. C., Natarajan, A., Jáuregui García, J. M., Peterson, J. B., & López-Cruz, O. 2014, ApJ, 782, L9
 Wieringa, M. H. 1992, Experimental Astronomy, 2, 203
 Zheng, H., et al. 2014, MNRAS, 445, 1084

APPENDIX

THE EFFECT OF REFLECTIONS AND CROSS-TALK ON VISIBILITIES

In this section, we develop formalism to discuss the impact of reflections of electromagnetic waves between antennas and within the signal chain of single antennas on foreground leakage in 21 cm experiments. We start with the time varying electric field from a single source with location $\hat{\mathbf{k}}$ on the sky, arriving at antenna i with delay τ_i and antenna j with delay τ_j with respect to the electric field at the origin which we denote as $s(t, \hat{\mathbf{s}})$. We allow for two different types of reflections: First, we allow reflections within the analogue path of each i^{th} antenna which we denote as $r_i(\tau, \hat{\mathbf{s}})$. We also allow for single reflections between any $i - j$ antenna pair which we denote as $r_{ij}(\tau', \hat{\mathbf{s}})$. Our choice of arbitrary τ' , for now, allows for multi-path propagation between antennas, though we expect it to be dominated by the geometrical delay between the antenna pair. The electric field at antenna i is given by

$$s_i(t, \hat{\mathbf{s}}) = \int d\tau' r_i(\tau', \hat{\mathbf{s}}) s(t + \tau_i - \tau') + \sum_{j \neq i} \int d\tau' s(t + \tau_j - \tau_{ij}) r_{ij}(\tau', \hat{\mathbf{s}}) \quad (A1)$$

In an FX correlator, the electric field is sampled, Fourier transformed, and cross multiplied between antenna pairs to form visibilities. The Fourier transform step leaves us with

$$\tilde{s}_i(f, \hat{\mathbf{s}}) = \tilde{s}(f, \hat{\mathbf{s}}) \left[\int d\tau' r_i(\tau', \hat{\mathbf{s}}) e^{2\pi i(\tau_i - \tau')f} + \sum_{j \neq i} \int d\tau' e^{2\pi i(\tau_j - \tau_{ij})f} r_{ij}(\tau', \hat{\mathbf{s}}) \right] \quad (A2)$$

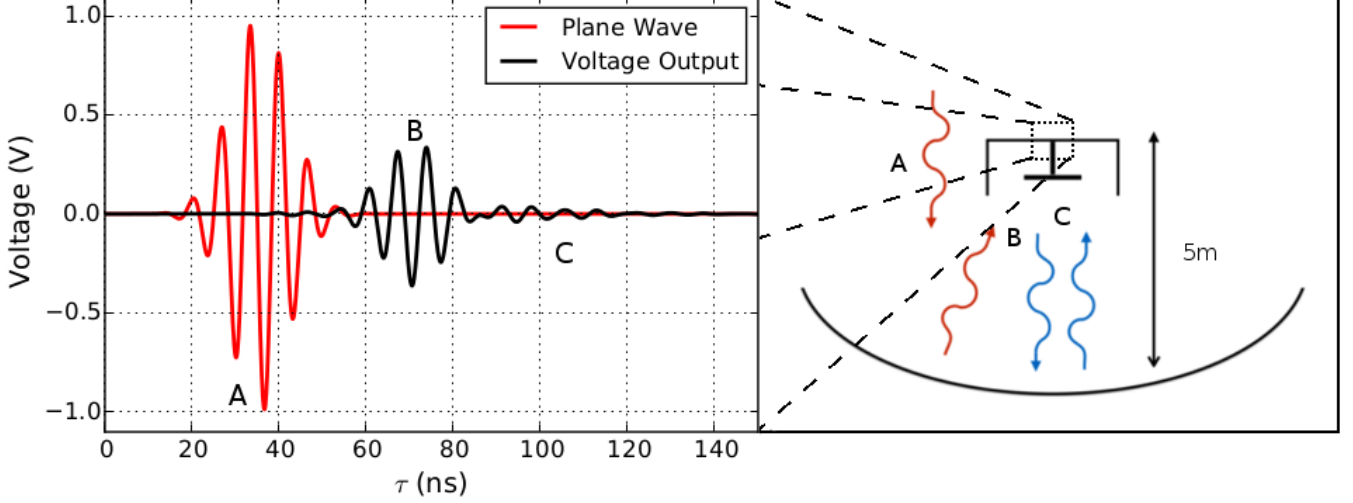


FIG. 3.— An illustration of our simulation products and their origin in the HERA antenna geometry. A plane wave is injected from above the feed (red line). The amplitude of the electric field of the plane wave at output of the feed along with the voltage at the feed terminal outputs is recorded (black line). The feed in our simulation is situated 5 m above the bottom of the dish, hence there is a ≈ 30 ns delay between when the plane wave passes the terminal for the first time (A) and when it is first absorbed in the dipole (B), leading to the voltage response. Of concern to 21 cm experiments are the subsequent reflections between the feed and the dish (C) which can lead to large delay contamination of the EoR window.

Multiplying and averaging gives us the visibility for the single source we obtain

$$\begin{aligned} v'_{ij}(f, \hat{\mathbf{s}}) &= \langle \tilde{s}_i(f, \hat{\mathbf{k}}) \tilde{s}_j(f, \hat{\mathbf{s}}) \rangle_t \\ &= d\Omega I(f, \hat{\mathbf{s}}) g_i(f) g_j^*(f) a_i(f, \hat{\mathbf{s}}) a_j^*(f, \hat{\mathbf{s}}) e^{2\pi i \mathbf{u}_{ij} \cdot \hat{\mathbf{s}}} + d\Omega I(f, \hat{\mathbf{s}}) \sum_{\ell \neq j} g_i(f) a_i(f, \hat{\mathbf{s}}) C_{\ell j}^*(f, \hat{\mathbf{s}}) e^{2\pi i \mathbf{u}_{\ell i} \cdot \hat{\mathbf{s}}} \\ &\quad + d\Omega I(f, \hat{\mathbf{s}}) \sum_{k \neq i} g_j^*(f) a_j^*(f) C_{ki}(f, \hat{\mathbf{s}}) e^{2\pi i \mathbf{u}_{kj} \cdot \hat{\mathbf{s}}} + d\Omega I(f, \hat{\mathbf{s}}) \sum_{k \neq i} \sum_{\ell \neq j} C_{ki}(f, \hat{\mathbf{s}}) C_{j\ell}^*(f, \hat{\mathbf{s}}) e^{2\pi i \mathbf{u}_{k\ell} \cdot \hat{\mathbf{s}}}, \end{aligned} \quad (\text{A3})$$

where $g_i(f) a_i(f, \hat{\mathbf{s}}) = \int d\tau r_i(\tau, \hat{\mathbf{s}}) e^{2\pi i f \tau}$ is the effective direction dependent gain of the system which can be factored into a direct-to-independently scattered radiation function where $g_i(f)$ is the gain of the analogue signal chain after the radiation has been absorbed by the feed and $a_i(f, \hat{\mathbf{s}})$ describes the chromatic electric field response of the antenna. The first term in equation A3 is an effective visibility with self-reflections. The two cross terms and the last term involve the mixing of visibilities complementary to the ij baseline and have the potential to introduce significant chromatic features since they potentially insert visibilities on much longer basline lengths. Assuming propagation along a single path directly between the antennas, we may write $C_{ik}(f, \hat{\mathbf{s}})$ as

$$C_{ki}(f, \hat{\mathbf{s}}) = a_i(f, \hat{\mathbf{s}}) \frac{1}{r_{ik}} \left[\frac{d\sigma_k}{d\Omega}(f, \hat{\mathbf{s}}, \hat{\mathbf{s}}_{ik}) \right]^{1/2} e^{2\pi i \tau_{ik} f} \quad (\text{A4})$$

Where r_{ik} is the distance between antennas i and k , $d\sigma_k(f, \hat{\mathbf{s}}, \hat{\mathbf{s}}_{ik})/d\Omega$ is the cross-section of the antenna to scatter radiation from the $\hat{\mathbf{s}}$ direction to the $\hat{\mathbf{s}}_{ik}$ direction where $\hat{\mathbf{s}}_{ik}$ is the unit vector in the direction between antenna i and antenna k . Integrating over the primary beam, we obtain a full expression on the effect of the foregrounds.

$$\begin{aligned} V'_{ij} &= \int d\Omega v'_{ij}(f, \hat{\mathbf{s}}) = g_i(f) g_j(f)^* \int d\Omega A_{ij}(f, \hat{\mathbf{s}}) I(f, \hat{\mathbf{s}}) e^{2\pi i f \mathbf{u}_{ij} \cdot \hat{\mathbf{s}}} + g_i(f) \sum_{\ell \neq j} \int d\Omega A_{i\ell j}(f, \hat{\mathbf{s}}) I(f, \hat{\mathbf{s}}) e^{2\pi i f \mathbf{u}_{\ell i} \cdot \hat{\mathbf{s}}} \\ &\quad + g_j^*(f) \sum_{k \neq i} \int d\Omega A_{jk i}^*(f, \hat{\mathbf{s}}) I(f, \hat{\mathbf{s}}) e^{2\pi i f \mathbf{u}_{kj} \cdot \hat{\mathbf{s}}} + \sum_{k \neq i} \sum_{\ell \neq j} \int d\Omega A_{kilj}(f, \hat{\mathbf{s}}) I(f, \hat{\mathbf{s}}) e^{2\pi i f \mathbf{u}_{k\ell} \cdot \hat{\mathbf{s}}} \end{aligned} \quad (\text{A5})$$

which is essentially an ad-mixture of many baselines with different effective primary beams. We denote the effective primary beam of the i, j antenna pair as $A_{ij}(f, \hat{\mathbf{s}}) = a_i(f, \hat{\mathbf{s}}) a_j^*(f, \hat{\mathbf{s}})$, the effective beam from a single reflection correlated with a direct measurement as $A_{i\ell j} = a_i(f, \hat{\mathbf{s}}) C_{\ell j}^*(f, \hat{\mathbf{s}})$ and the correlation between entirely reflected terms as experiencing an effective primary beam of $A_{kilj} = C_{ki}(f, \hat{\mathbf{s}}) C_{j\ell}^*(f, \hat{\mathbf{s}})$. In this paper, we focus on the reflection terms within a single antenna element. Hence, we ignore all but the first term for now. Any reflection terms occurring downstream of the conversion by the feed from electromagnetic radiation to voltage are lumped into $g_i(f)$ and reflections occurring within the antenna element enter into $a_i(f, \hat{\mathbf{s}})$. While reflections within the analogue system are a potential source of contamination, HERA's post-feed analogue signal path is designed to keep all reflections under 35 m, within the wedge.

The focus of this paper and its companions is the reflection properties of the primary antenna element, so we will focus the rest of our discussion here on $a_i(f, \hat{\mathbf{s}})$. The primary elements of our dish include a feed and backplane suspended over a fourteen meter dish. We assume a set of discrete reflections within the dish, which without loss of generality are assumed to have frequency independent reflection coefficients⁷ hence

$$a_i(f, \hat{\mathbf{s}}) = \sum_n r_n(\hat{\mathbf{s}}) e^{2\pi i \tau_n f} \quad (\text{A6})$$

Assuming all antennas are identical, we have

$$A_{ij}(f, \hat{\mathbf{s}}) = \sum_m \sum_n r_n(\hat{\mathbf{s}}) r_m^*(\hat{\mathbf{s}}) e^{2\pi i (\tau_n - \tau_m) f} = \sum_\alpha A_\alpha(\hat{\mathbf{s}}) e^{2\pi i \tau_\alpha f} \quad (\text{A7})$$

where we have re-indexed m and n under a single greek index α in the second equality. The effect of internal reflections on a visibility is hence

$$V'_{ij} = \sum_\alpha \int d\Omega A_\alpha(\hat{\mathbf{s}}) e^{2\pi i \tau_\alpha f} e^{2\pi i \mathbf{b}_{ij} \cdot \hat{\mathbf{s}} f / c} I(f, \hat{\mathbf{s}}) \quad (\text{A8})$$

Taking the delay transform, one obtains

$$\tilde{V}'_{ij}(\tau) = \sum_\alpha \tilde{V}_{ij}^\alpha(\tau - \tau_\alpha) \quad (\text{A9})$$

where

$$\tilde{V}_{ij}^\alpha(\tau) = \int d\tau e^{-2\pi i f \tau} \int d\Omega A_\alpha(\hat{\mathbf{s}}) e^{2\pi i \mathbf{b}_{ij} \cdot \hat{\mathbf{s}} f / c} I(f, \hat{\mathbf{s}}) \quad (\text{A10})$$

is the usual delay transform of Parsons et al. (2012). $\tilde{V}_{ij}^\alpha(\tau)$.

⁷ If we allow each coefficient to be frequency dependent, we can expand each frequency dependent term in a Fourier series of frequency independent terms